INTERNATIONAL JOURNAL OF GREEN ENERGY
2023, VOL. 20, NO. 10, 1086–1100
https://doi.org/10.1080/15435075.2022.2143715

Taylor & Francis
Taylor & Francis Group

Modeling and performance evaluation of sustainable arresting gear energy recovery system for commercial aircraft

Jakub Deja, Iman Dayyani, and Martin Skote

School of Aerospace, Transport and Manufacturing, Cranfield University, Cranfield, UK

ABSTRACT

A significant amount of kinetic energy is dissipated during each commercial aircraft landing. To improve energy efficiency and environmental sustainability, the kinetic energy can instead be converted to electricity by utilizing the arresting gear systems. This paper presents a novel design that couples an arresting gear system to electrical generators. The results show that the system can successfully recover aircraft kinetic energy and is applicable to different aircraft sizes ranging from Airbus A319 up to A380. Beyond system performance, wider context technical aspects including system integration into grid with multiple energy storage possibilities, safety and passenger comfort are discussed.

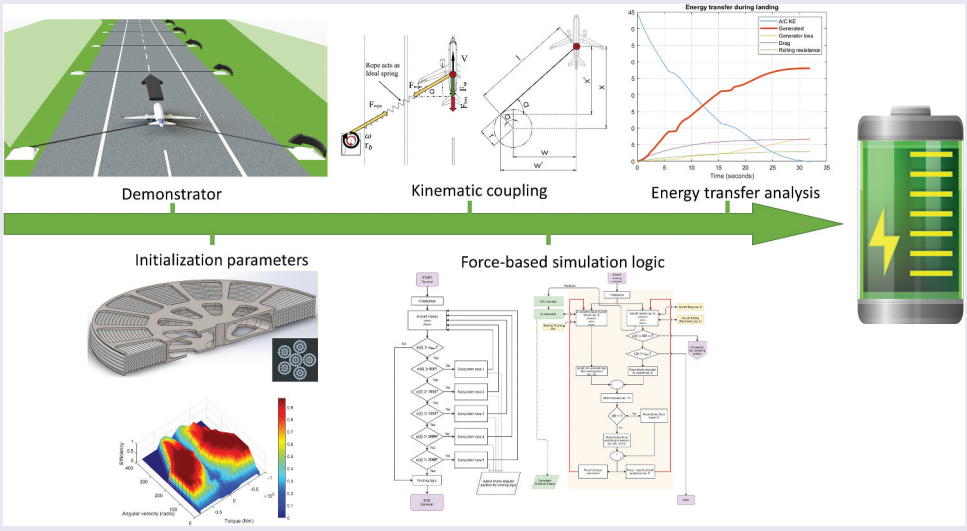

ARTICLE HISTORY
Received 16 June 2022
Accepted 21 October 2022

KEYWORDS
Commercial Aircraft; Kinetic Energy Recovery; Arresting Gear; Landing Phase

1. Introduction

One of the biggest concerns of the aerospace industry is sustainability. The pollution from aircraft is expected to be 7 to 10 times higher in 2050 compared to 1990 level (European Parliament 2019) and long-term projections indicate that aerospace will be the cause of the highest percentage increase in total greenhouse gas emissions. Plans to address this issue include an International Civil Aviation Organization (ICAO) target to decrease annual fuel consumption by 2% up to 2050 (Fleming and de Lepinay 2019). The European Parliament similarly proposes the 'Flightpath 2050' project where besides reducing overall greenhouse gas emissions, one of the key points is emission-free taxi movement (European Commission 2011). Lee et al. (2021) defined emissions and noise as the environmental impact factors of air transport and they consider the ground operations as the contributing aircraft mission phases. The organization targets to optimize the aircraft ground operations by implementing zero emissions taxiing and improving fuel burn on ground. Apart from the aerospace industry, different organizations also indicate the necessity for green and sustainable energy solutions. United Nations (2022) strive with their seventh goal to ensure access to affordable, reliable, sustainable and modern energy for all. Engineering and Physical Sciences Research Council (2019) emphasized the objective for new energy technologies in their 2019 delivery plan.

Aircraft manufacturers respond to the calls for sustainable aviation by improving key aircraft parts and systems and the following actions are being taken: (a) development of more efficient propulsion at cruise phase (Epstein 2014); (b) introduction of sustainable aviation fuels (Yilmaz 2022); (c) increasing use of composite materials in aircraft to reduce weight

CONTACT Jakub Deja jakub.deja@cranfield.ac.uk School of Aerospace, Transport and Manufacturing Cranfield University, College Road, Cranfield MK43 0AL, UK

(Zolkin, Galanskiy, and Kuzmin 2021); (d) changes in aircraft aerodynamic shape to improve glide performance (Abbas, de Vicente, and Valero 2013; Lauk 2019) and (e) augmentation of avionics with 4-D flight trajectory optimization technology (Liu et al. 2021). Similarly, sustainable systems are being developed for airport operations to minimize the usage of aircraft propulsion due to its relative inefficiency during taxiing (Kottas, Bozoudis, and Madas 2020). The up-to-date development includes the aircraft towing undercarriage systems (TaxiBot 2021) and electric taxiing (Safran 2017; WheelTug 2021). These systems source energy from either an aircraft's Auxiliary Power Unit (APU) or from a tug's batteries. However, little research has been done toward reducing landing phase emissions which occur when the reverse thrust system is engaged. Openairlines (2021) estimate fuel consumption difference of up to 60 kg between maximum thrust reverse and idle thrust reverse for Airbus A380. The wear of brake discs and pads also contributes to emissions due to release of the fine component particles (Masiol and Harrison 2014).

A landing aircraft holds a significant amount of kinetic energy due to its mass and velocity. Currently, most of this energy is dissipated as heat whereas, if captured, it can be converted into electrical energy and used for airport operations. Therefore, the requirement is set for an additional deceleration system producing enough power to decelerate an aircraft at standard rate and harvest as much energy as possible during an operation. The military arresting gear technology is proven to work on aircraft carrier decks and in emergency situations but is used only for stopping an aircraft without recovering kinetic energy (Wu et al. 2017). The USS Navy aircraft carriers have had the Mark 7 Mod 3 arresting gear system installed (Eggleston 2011), which is capable of stopping a fighter jet at a distance of up to 105 m.

An arresting cable is subjected to the toughest operating conditions due to high impact during contact with an arresting hook and dragging on runway. The military system utilizes two types of cables. The 'deck pendant' is a smaller diameter steel wire rope which catches the arresting hook while the 'purchase cable' is a bigger diameter rope and is used to translate the force from deck pendant to arresting engine. Alternatively to steel wire ropes, the BAK-12 military arresting gear system utilizes tape in place of the 'purchase cable' (Adamowicz, Poświata, and Wesołowski 2021).

This paper proposes for the first time a similar system to that used in the military, but one augmented with powerful motor-generators to enable the production of electricity. The large power generator applications include hydroelectric and wind turbines. The largest dam on earth, Three Gorges Dam, utilizes the electric machines capable of producing 700 MW rated power each (Gleick 2009). One of the largest offshore wind turbines, Vestas V236, has a rated power equal to 15 MW (Vestas 2021). Commercial aircraft vary by size depending on the application but the rated power of hydropower generator is much greater than that needed to stop even the largest aircraft, Antonov AN-225, at a standard landing distance. The demonstrator design incorporates a gear reducer which is used for energy efficiency optimization. A dynamic model was used to simulate the energy transfer between the system and the airline aircraft. The results allow for investigation of the forces acting during operation and estimation of the electrical energy produced from each landing.

Table 1. Experimental rolling resistance coefficient for Boeing 737 tyres (Yager, Stubbs, and Davis 1990).

Velocity (m/s)	Rolling resistance coefficient
3	0.01
51	0.014
82	0.025

2. Standard landing procedure review

Implementation of the new system requires an understanding of standard landing procedure for all aircraft that are involved in an arresting process. The system proposed in this paper suits various commercial aircraft sizes, from Airbus A319 to Airbus A380. The stopping distance and deceleration are safety critical parameters due to runway excursion risk and additionally, severe deceleration may cause passenger and flight personnel discomfort. Hence, the objective has been set to maintain similar values to those during a normal landing. Rustenburg, Skinn, and Tipps (2002) gathered telemetric data for Airbus A320 with a statistical sample equal to 10066 flights where landing gross mass varied between 47 and 65 metric tons and touchdown airspeed remained in the envelope between 56 and 78 m/s. The maximum velocity during a touchdown is limited by the tyre certification. An overhaul specialist company, RotableRepairs (2021), stated that maximum Airbus A320 tyre speed equals approximately 100 m/s. Aircraft braking during a landing roll is nonlinear and dependent on multiple parameters. The highest deceleration value occurs when the thrust reverses are engaged and equals on average to 1.962 and 5.40 m/s^2 maximum (Rustenburg, Skinn, and Tipps 2002). Airbus A320 Flight Crew Operating Manual (Openairlines 2021) provides the stopping distance values between 679 and 4742 m. The exact value is influenced by aircraft gross weight, airfield elevation as well as wind and weather conditions. Furthermore, Airbus Aircraft Characteristics for Airport and Maintenance Planning Airbus (2005a, 2005b) provide dry runway condition airfield length ranging from 914 m for Airbus A319–100 to 2700 m for Airbus A380–800.

The total kinetic energy of aircraft during landing roll available to recover is given by:

$$\Sigma KE = \frac{1}{2}mv^2 + \Sigma\frac{1}{2}I\omega^2 \quad (1)$$

where m is the mass of the aircraft, v is the resultant ground speed of an aircraft, I is the moment of inertia and ω is the angular velocity of landing gear rotary components. During a landing roll, the aircraft is continuously subjected to drag which can be divided into parasitic and induced drag. Induced drag is assumed to be negligible whereas parasitic drag equation formula is given as:

$$F_D(t) = C_D \times A \times \frac{\rho v_a(t)^2}{2} \quad (2)$$

Table 2. Aircraft parameters used as initial conditions in dynamic simulation, nominal landing distance provided for reference (Airbus 2005a, 2005b; ModernAirlines 2021; Palt 2019; Rustenburg, Skinn, and Tipps 2002).

Airbus aircraft for reference	Landing Gross Weight (metric tons)	Total wing area (m^2)	Drag Coefficient	Arresting Ground Speed (m/s)	Landing Distance (sea-level, International Standard Atmosphere) (m)
A318	57	123	0.116	68	1200
A319	61	124	0.116	68	1300
A320	64.5	125	0.12	68	1400
A321	77.8	128	0.133	68	1600
A332	180	362	0.118	68	1800
A333	182	362	0.12	68	1800
A340	192	430	0.12	68	1900
A350	205	440	0.12	68	1900
A359	233	443	0.12	68	1900
A380	386	845	0.104	68	2200

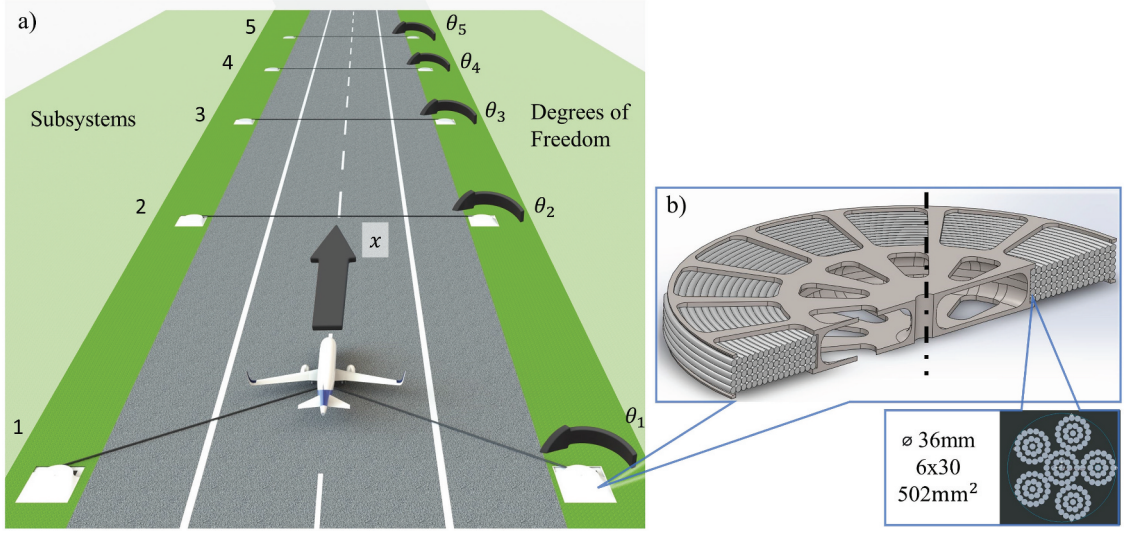

Figure 1. Arresting gear system demonstration showing arresting process, cross-section of underground installation and related degrees of freedom used in dynamic simulation. a) Arresting process graphic demonstrator b) Winding drum and steel wire rope cross-section.

where F_D is the drag force, C_D is the drag coefficient, A is the reference area, ρ is the air density and v_a is the relative airspeed. The drag coefficient values are sourced from Sun, Hoekstra, and Ellerbroek (2020) who developed a stochastic hierarchical model in order to provide aerodynamic coefficients reflecting landing gear and flaps extension for multiple aircraft.

The rolling resistance has been modeled as:

$$F_{rr}(v) = \mu(v) \times mg \tag{3}$$

where F_{rr} is a force acting opposite to aircraft moving direction, μ is a coefficient of rolling resistance, m is an aircraft mass and g is a gravitational acceleration. Yager, Stubbs, and Davis (1990) gathered experimental data for 40×14–19 tyres dedicated to similar aircraft such as Boeing 737. Table 1 shows μ values which were captured at 2.6, 51.4 and 82.3 m/s.

The rolling resistance coefficient values were used as breakpoints that were later linearly interpolated to match exact aircraft velocity at given time increment.

None of the landings are exactly the same due to varying aircraft landing gross weight and ground speed during touchdown. An aircraft manufacturer always provides the acceptable range for the landing parameters. Table 2 shows the exact initialization parameters values used in simulation iterations, which are in the standard landing procedure interval.

3. Idealized arresting gear cable system

The proposed design is fitted onto a runway with footprint dimensions similar to London Heathrow southern runway (Heathrow Airport Ltd 2021). The arresting process visualization, and winding drum assembly cross-section view are available in Figure 1.

Unlike military applications where a single cable is used for the short distance landing on a flight deck, the landing of civil aircraft at the size of the Airbus A380 and standard deceleration and distance requires the sequential cables coupled to generators. Figure 1a shows that the whole arresting gear system fitted on the runway consists of five arresting cables where each is winded onto two drums located at each side of the runway. When the aircraft rolls over a cable, the arresting hook catches it and pulls the winding drum inducing a generator rotor angular motion. As soon as the aircraft passes 30 m distance from the arresting point, a generator control system applies counteracting torque that slows down the aircraft.

Most components remain underground to maximize safety in case of runway excursion by allowing aircraft to roll over the enclosure without any damage. The system protrudes above soil by less than one meter and the safety enclosure separates the wheels from all the sharp components. The detailed cross-section view of each subsystem

presenting the components under enclosure is available in Appendix A.

3.1. Arresting gear cable

Knowing that the Mark 7 Mod 3 system was suited for the F-14D Tomcat (Eggleston 2011), it is possible to estimate how much force was applied to the cable. The aircraft maximum allowable gross landing weight equals approximately 20 metric tonnes and short-field landing maximum speed equals to 82 m/s (Department of the Navy 2004). Assuming linear deceleration, the cable in the Mark 7 Mod 3 arresting system is subjected to a force described by the following kinematic equation:

$$F_{rope} = m \times \frac{v^2 - u^2}{2s} \tag{4}$$

where m is mass of aircraft, a v is initial velocity, u is final velocity and s is a path traveled. After substituting variables with values for the F-14D Tomcat, there is 640 kN tension applied to the cable.

Each winding drum can allocate up to 500 m of arresting cable raising the concern about corresponding mass and moment of inertia. Approximate mass for 36 mm diameter steel wire rope used in Mark 7 Mod 3 was estimated at 5.3 kg/m (SWR 2021). In dynamic model, the cable acts as a spring and its cross-sectional area and length affects spring stiffness. As presented in Figure 1b, the cross-section area estimate has been made in CAD software and is equal to 502.55 mm^2 for 6×30, 36 mm diameter steel wire rope. The detailed arresting cable parameters are available in Appendix B. The steel wire rope loses its mechanical strength when bent. The Crosby Group (2013) provided data where they state that bending a rope on sheave with diameter 40 times greater than a rope diameter results in 95% of nominal rope strength. Hence, the minimum diameter for all sheaves and winding drums used in the proposed system is equal to 1440 mm.

3.2. Coupling between aircraft and winding drum subsystem

The arresting process is idealized and consequently limits aircraft motion to only one axis. The aircraft kinematics are described by:

$$\ddot{x}(t) = \frac{\sum \vec{F}(t)}{m} \tag{5}$$

where x is the aircraft position, $\sum \vec{F}$ is the resultant force acting in x-axis and m is the mass of aircraft. Similarly, the angular drum kinematics are described by:

$$\ddot{\vartheta}(t) = \frac{\sum \vec{M}(t)}{I} \tag{6}$$

where ϑ is the drum angular position, $\sum \vec{M}$ is the resultant momentum and I is the moment of inertia for each subsystem. The dynamic model has six degrees of freedom where the first one is a moving aircraft and the rest are winding drums. Since the model is symmetrical, only one side is considered in simulation with doubled moment of inertia. An arresting cable acts as a spring where the strain is calculated by subtracting a length released from the winding drum from a cable length projection driven by an aircraft position. Figure 2 shows the kinematic coupling between the arresting gear system and constrained motion of aircraft. All the variables are presented in the figure.

where ω is the angular velocity of winding drum, τ_b is the negative torque due to bearing friction, F_{rope} is the force translated through the cable, F_{ag} is the force projected on the aircraft, V is the aircraft velocity, w is the distance from sheave to center of runway, w′ is the *w* corrected with tangential point

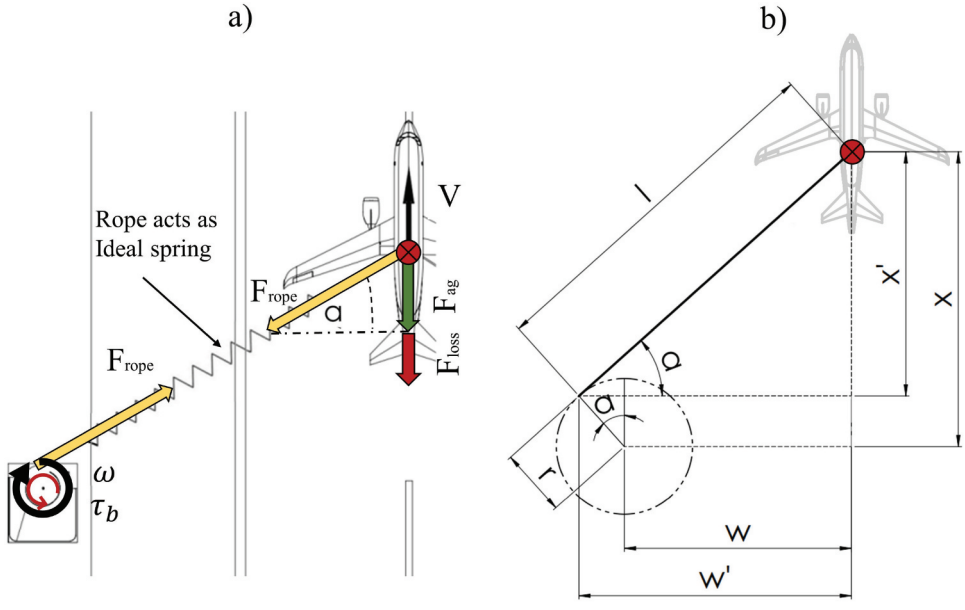

Figure 2. Split view between free body diagram and winding drum aircraft coupling kinematics annotated with dimensions.

displacement, x is the distance passed by aircraft from arresting point and x′ is x corrected with tangential displacement, l is the length of free cable, α is the angle between a cable and a runway axis.

Assuming that x and w are known at each time step, $\alpha(t)$ can be found by the following kinematic relations:

$$(m/s) \tag{7}$$

The system has multiple real solutions but knowing that $\alpha \in [0, 90^\circ)$, there is only one solution in given quadrant. Thus, the system can be rewritten as an angle function of x travel, where the only variable is aircraft travel in x-axis:

$$\alpha(x) = -2 \times \arctan \frac{w - \sqrt{-r^2 + w^2 + (x(t) + r)^2}}{x(t) + 2r} \tag{8}$$

Once the angle is known, the distance from winding drum tangential point to aircraft hook can be estimated as:

$$\delta l_a(t) = (w + r \sin \alpha(t)) \times \cos \alpha(t) \tag{9}$$

while length of cable released from the sheave described is by:

$$l_r(t) = \sum^{t} \delta\vartheta(t) \times r(t) \tag{10}$$

The spring strain at each time increment is:

$$l_s(t) = \delta l_a(t) - l_r(t) \tag{11}$$

Hence, the force can be estimated according to Hooke's law:

$$F(t) = -k(t)x(t) \tag{12}$$

where spring constant is derived from Young's Modulus and can be calculated from:

$$k(t) = \frac{\Delta F(t)}{\Delta A} = \frac{EA}{L(t)} \tag{13}$$

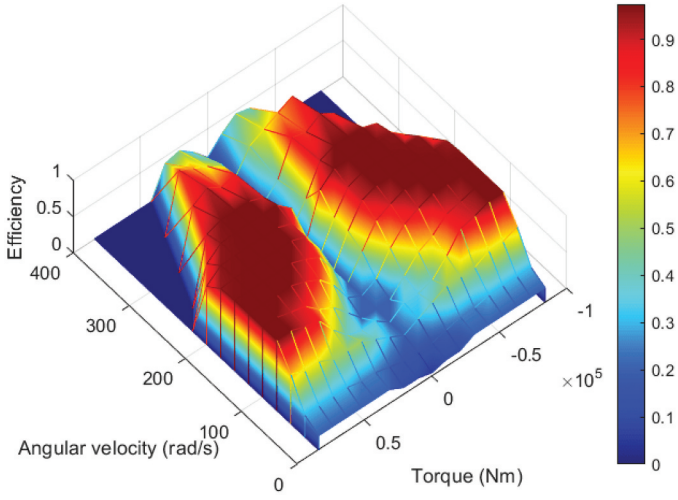

Figure 3. Motor-generator efficiency map against different torque and angular velocity values.

3.3. Electric machines

The system requires powerful generators producing enough torque to slow down an aircraft at a demanded deceleration rate. The peak generator power is required for the heaviest aircraft during the initial arresting stage. Airbus A380 at maximum landing weight is equal to 386 metric tons and rolling at 68 m/s. The aircraft has to decelerate at approximately 1.3 m/s^2 and that power in simplified cases equals to force times velocity, Airbus A380 requires as much as 34 MW of power to slow down at given deceleration rate. There are two generators for each subsystem. Hence, the power required for each generator should be halved and consequently is equal to 17 MW.

The generator was chosen regarding this demand for peak power and also regarding maximum angular velocity which was driven by an aircraft landing speed, a winding drum radius and a gear reduced gear ratio. Siemens (2021) offers large size industrial motors and provides a datasheet with efficiency for four power loads. Nonetheless, this analysis requires accuracy higher than four power breakpoints while the whole efficiency map is commercially sensitive. Theoretically, each motor can work as a generator with similar performance and therefore, assumption is made that efficiency curve is symmetrical for negative and positive torque. Figure 3 shows the efficiency estimates for whole torque and angular velocity envelope. The approximation was made by scaling the values from Kumar (2015) and Badain et al. (2015). They provided the motor-generator data for their energy recovery applications.

The parallel gear reducer was selected rather than a right-angled alternative because of the higher efficiency at a price of the greater geometric footprint corresponding to parallel coupling. The off the shelf gearbox that matches the load requirements was found (Nord Drivesystems 2021). According to the datasheet, the proposed gear reducer has 97% efficiency. The control architecture for motor-generator was designed with the assumption that aircraft longitudinal deceleration is known. The feedback can be captured either by remote connection to an aircraft's inertial measurement unit (IMU) or by ranging devices.

3.4. System moment of inertia

During the initial stage of the arresting process, the aircraft translates its momentum via a cable to the stationary arresting gear system. The system resists due to the rotary components moment of inertia and is reflected to aircraft as slowing down force. If torque becomes excessive, the resultant aircraft deceleration will be too high. One way of reducing this issue is to use a motor-generator to induce rotation. However, there is a risk of motor-generator failure which may lead to excessive loads on both the system and the aircraft. Instead, the problem was resolved by keeping the moment of inertia value small enough. Once the maximum value was known, the suitable components were selected. Table 3 shows the major components contributing to overall moment of inertia.

The span between drums equal approximately 120 m and the cable laying on the runway weighs 630 kg which equals to approximately 1% of an Airbus A320 aircraft gross landing weight. Hence, the inertia of the cable across the runway at an initial stage of arresting process was neglected.

Table 3. Moments of inertia of each subsystem.

Component	Moment of Inertia reflected to aircraft (kgm^2)	Quantity
Motor-Generator	1900 (Siemens 2021)	2
Gear Reducer	96 (Nord Drivesystems 2021)	2
Winding drum	1490	2
Winded cable	768	2
Total for a subsystem	8508	

The moment of inertia for most components is provided in suppliers' datasheets. Nevertheless, the design assumes a bespoke winding drum with moment of inertia estimated in CAD environment including the winding drum itself and approximately 500 m of winded cable. Figure 1b presents the winding drum cross-section view across centreline with rope winded onto it.

3.5. Winding process

Aircraft land or take-off every forty five seconds on busy airports such as London Heathrow (Airport Technology 2020) requiring the arresting gear system to offer an efficient and automated cable winding system. The major energy loss factor during the winding process are motor efficiency and cable dragging along the runway represented by:

$$F_{friction}(t, v) = m_r \times l(t) \times g \times C_f(v) \quad (14)$$

where m_r is mass of cable per meter, g is gravitational force and C_f is coefficient of friction between runway and cable. The friction model is dependent on dragging velocity and combines Coulomb friction, Stribeck effect and Viscous Friction (Yang, Yang, and Ding 2018). The friction occurs between steel and concrete where static and dynamic coefficients equal 0.57 (Rabbat and Russell 1985) and 0.38 (Engineers Edge LLC 2021) accordingly. The graph showing coefficient of friction against a dragging velocity is available in Appendix B.

3.6. Energy storage

Similarly to photovoltaic and wind farms, there is a problem of high intermittent power that is difficult to integrate with the grid (Li et al. 2022; Zsiborács et al. 2019). An aircraft decelerates within less than a minute while generating up to 140 kWh of energy. Thus, an energy storage system must be implemented wherein batteries and supercapacitors are considered. Steilen et al. (2015) stated that a round conversion efficiency for a battery remains between 70% and 95% while Barrade and Rufer (2004) defined the efficiency of a supercapacitor reaching nearly 100%. The supercapacitors are more appropriate for the arresting gear system because energy has to be stored only for a short period of time between aircraft landings, downsizing the self-discharge issue. Furthermore, the charge rate would be sufficient unlike with the Li-Ion batteries which are subjected to degradation processes at higher rates (Tomaszewska et al. 2019). A major drawback is the cost of installation which is equal to approximately $10,000 per kWh Feldhan (2019). Nevertheless, it is suggested that the new technologies utilizing graphene and carbon nanotubes will reduce unit price in the future (The Business Research Company 2020). Finally, Song et al. (2018) proposed a battery-supercapacitor hybrid solution for electric vehicles that sums up functionalities of both and result in reduced overall costs of implementation.

The hydro pumped storage may be considered as an alternative solution. Anagnostopoulos and Papantonis (2007) proposed a wind-hydro design which can be altered so a pump would be connected directly to the arresting gear generators and work at a high power for a limited time. This solution could be particularly feasible for London Heathrow airport due to its close proximity to Staines reservoir.

4. Simulation and results

To validate the arresting gear concept, a simulation was initialized with parameters given in Section 3 and the set of differential equations was analyzed in time domain using MATLAB/Simulink software. The idealized dynamic model assumes (a) a rigid airframe with the weightless rotational components, (b) a rigid winding drum, (c) an arresting cable acting as a spring, (d) idealized generator dynamics, (e) six degrees of freedom, (f) degrees of freedom consisting of aircraft linear motion and five subsystems angular motion, (g) an aircraft aligned perfectly with centreline, (h) aerodynamics accounting to drag only (neither lift nor downforce) and (i) International Standard Atmosphere (ISA) flight condition at sea level. Figure 4 presents The top-level simulation logic flowchart.

If velocity of an aircraft achieves the demanded taxi velocity v_{taxi}, the simulation ends. Otherwise, the process runs until the aircraft travels 2500 m from the beginning of the arresting process while changing the arresting subsystem at 500 m aircraft travel distance increment. The control logic was set to reduce the cable tension after 430 m aircraft travel distance within each subsystem in order to safely release a cable. The motion data from each subsystem is saved and later used as initialization for winding logic. Figure 5 presents the subsystem flowchart and details a coupling between an aircraft and a winding drum.

The yellow colored area corresponds to two degrees of freedom, aircraft linear motion and winding drum angular motion, which are coupled with a spring that translates forces only due to tension. If compression occurs, there is no force acting between two degrees of freedom because the cable will bend sideways. There are five energy loss factors. The winding drums lose energy due to bearing friction, while the aircraft itself dissipates kinetic energy due to drag and rolling resistance. The generator efficiency is affected by mechanical (friction), hysteresis, eddy current and ohmic phenomena, while the gear reducer is subjected to mechanical losses only (Masuzawa, Osa, and Mapley 2018). Finally, most of the energy is converted to electricity through generators that apply torque corresponding to aircraft deceleration feedback. The winding process uses the generated

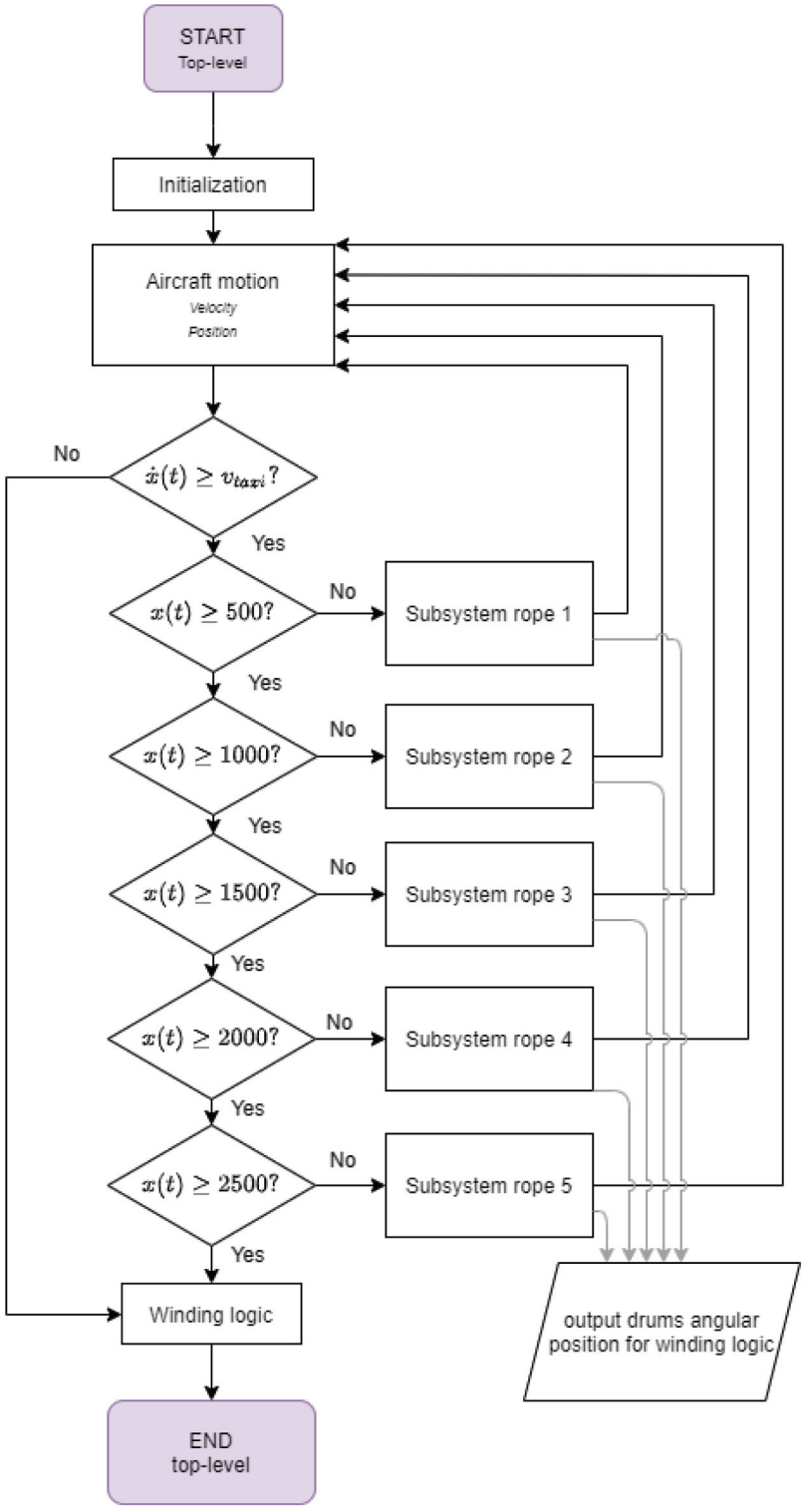

Figure 4. Top-level simulation flowchart logic explaining runout breakpoints.

electrical energy to wind back the rope and make the system available for the next aircraft. Figure 6 presents the winding simulation flowchart which consists of one degree of freedom.

An additional energy dissipation factor, a rope dragging on runway, is simulated by estimating the cable on runway mass multiplied by coefficient of friction with regards to dragging velocity given in A ppendix C. The simulation results show that the proposed large motor-generator has very low efficiency equal to approximately 20% during the winding process due to the application of negligible loads. Hence, the alternative solution consisting of another, smaller motor coupled to each winding drum with a mean efficiency equal to 85% is proposed. Figure 7 shows motion, forces and energy transfer during arresting of Airbus A320.

As can be seen in Figure 7a, the actual aircraft deceleration matches the demanded signal (R1 dem, R2 dem, R3

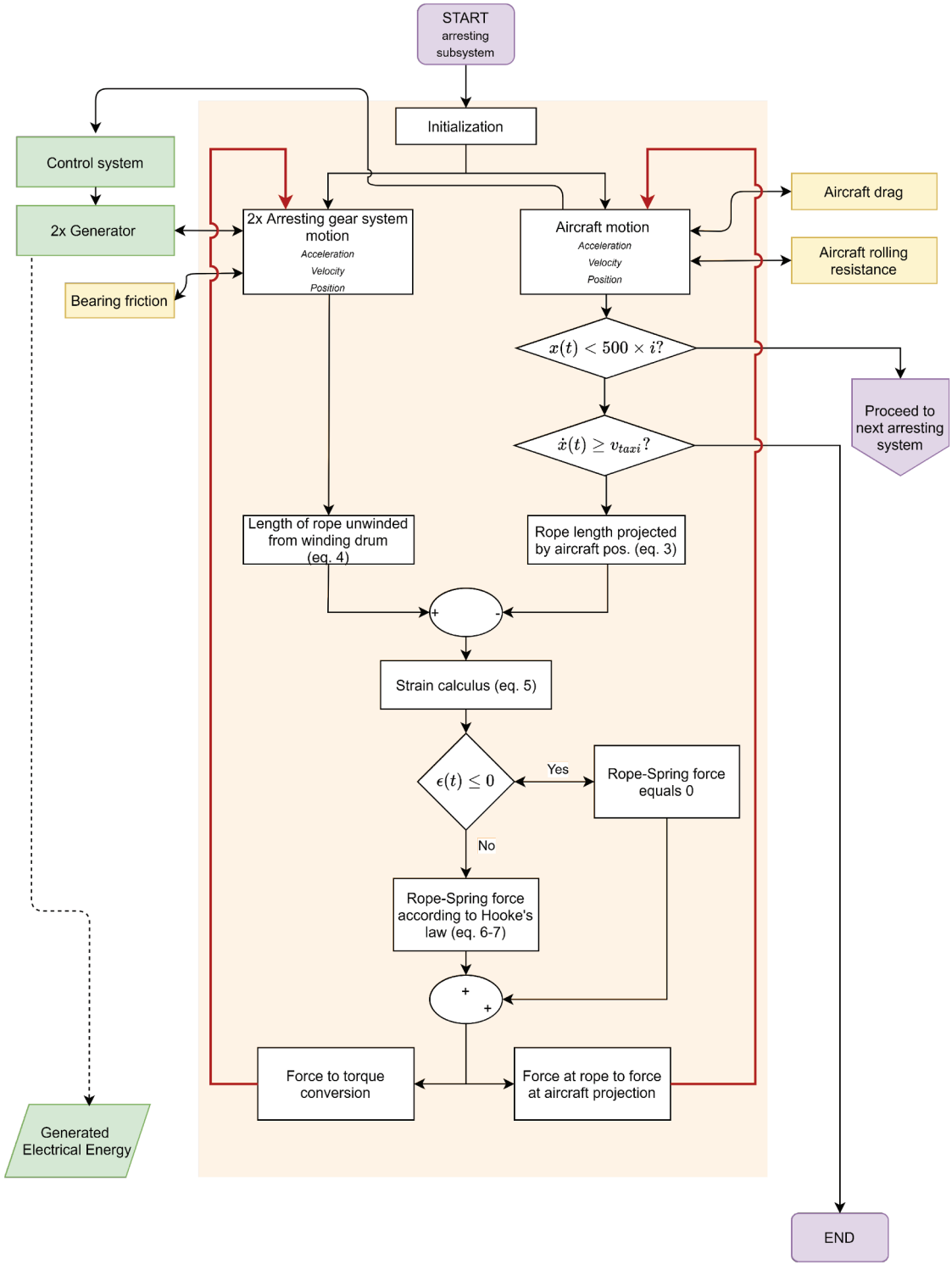

Figure 5. Arresting gear subsystem flowchart logic showing a coupling between aircraft and winding drum and energy loss factors.

dem) due to the idealized control architecture with an instantaneous response. There is a small disturbance within all subsystems caused by a variable radius logic. The system response indicates that generators produce enough power to meet the application requirements. Figure 7b shows that the aircraft stops in approximately 32 secs after passing 1100 m. The distance matches the aircraft manufacturer data specification (Airbus 2005b). The force translated through the first cable in Figure 7c reaches 40 metric tons, which fits the rope tensile strength envelope and remains lower than during an F14-D Tomcat landing on an aircraft carrier. The first and second system presented in Figure 7d works at nearly constant angular velocity due to variable radius of a released rope. The winding drums angular velocity varies between 45 and 0 rad/s. As presented in Figure 7e, the system generates approximately 27 kWh of energy but uses 2 kWh for winding the rope back. Thus, the energy efficiency equals approximately 60%. Other

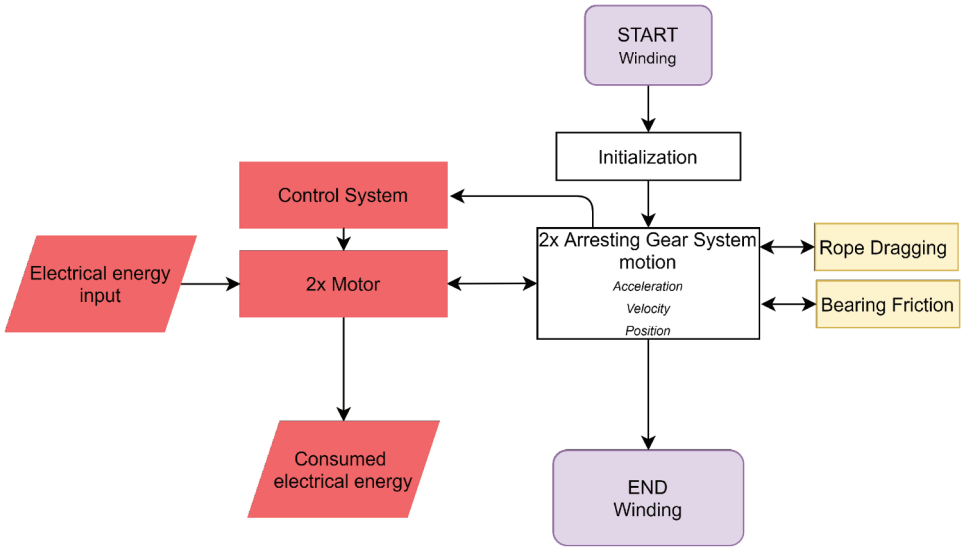

Figure 6. Winding flowchart logic showing energy transfer to wind up each subsystem.

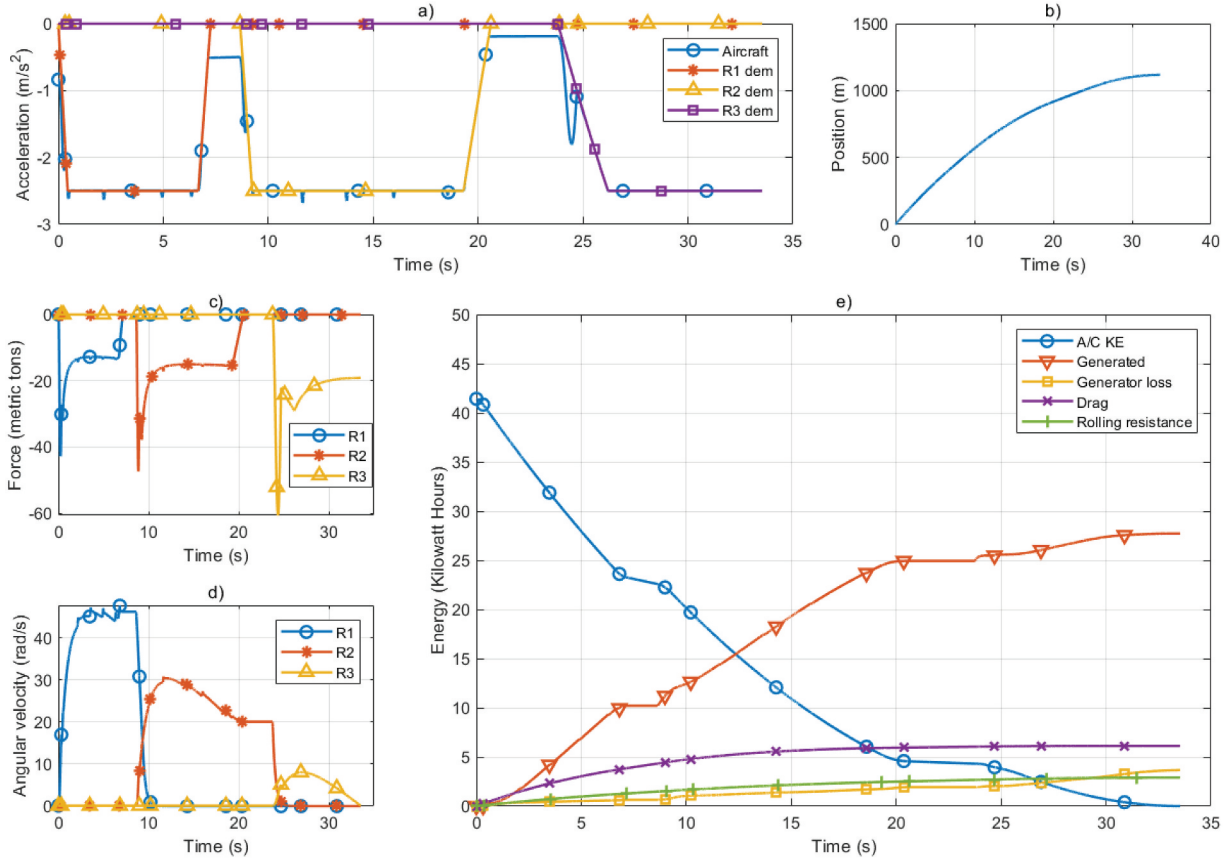

Figure 7. Airbus A320 results showing motion of aircraft along with all involved arresting subsystems and forces acting on a rope during landing. (a) Aircraft acceleration, (b) Aircraft position, (c) Rope tension, (d) Subsystems angular velocity, (e) Energy transfer during landing.

iterations were conducted according to initial conditions from Table 1 and are presented in Table 4.

The efficiency varies between different aircraft where the highest is achieved with medium weight aircraft and tends to drop for heavier and lighter aircraft. The stopping distance for all remains within the standard landing envelope so is the peak deceleration. Deceleration for the smallest aircraft is driven by system moment of inertia. As the aircraft mass increases, the peak deceleration reduces. The number of subsystems engaged is increasing with the weight of aircraft due to limited generator power and runout distance. The graphs related to data from Table 4 are available in Appendix C.1 showing the energy transfer and in Appendix C.2 providing the stopping distance and the amount of recovered energy for all iterations.

The simulation results were validated according to the law of conservation of energy. The aircraft kinetic energy

Table 4. Simulation results for aircraft ranging from Airbus A318 to A380.

Aircraft for reference (IATA code)	Kinetic energy available (kWh)	Amount of energy stored in supercapacitors (kWh)	System efficiency %	Stopping distance (m)	Peak deceleration (m/s^2)	Number of arresting gear subsystems engaged
A318	37	21	57	1050	2.8	3
A319	39	24	62	1070	2.7	3
A320	41	25	61	1100	2.6	3
A321	50	34	68	1150	2.6	3
A332	116	67	58	1350	2.1	3
A333	117	67	57	1400	2.0	3
A340	123	64	52	1600	1.7	4
A350	132	67	51	1700	1.6	4
A359	150	75	50	1850	1.4	4
A380	248	110	44	2200	1.2	5

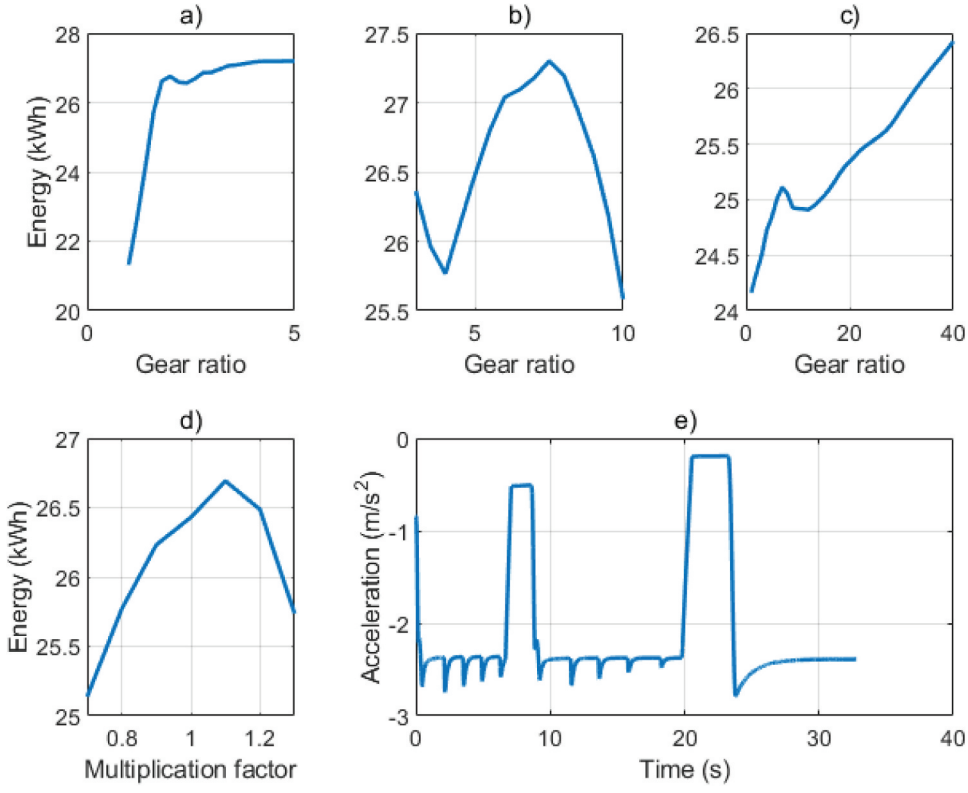

Figure 8. Gear ratio optimization results performed for Airbus A320. (a) Optimization of first subsystem, (b) Optimization of second subsystem, (c) Optimization of third subsystem, (d) Optimization of all subsystems combined, (e) Aircraft response for optimized setup.

and all energy dissipation factors were summed up and investigated throughout the simulation time. The results shown that the total energy variance of the dynamic model equals 0.1% of the total energy. This negligible error is caused by the multiple logical operators, the variable winding drum radii and the numerical inaccuracy. Furthermore, the kinematic coupling between the system and a landing aircraft has been validated with the hand calculus at several different angles.

5. System optimization based on parametric study for airbus A320

The proposed system consists of multiple components that affect the overall energy transfer efficiency. Better performance can be achieved by optimizing factors such as a radius of winding drum, where the adjustment allows to use the highest-efficiency torque and angular velocity ranges of generator. The solution is mostly applicable if direct drive design is chosen, but the adjustability is limited by bending radius of a cable and a system moment of inertia reflected to the rope. If a gear reducer is present in a system, optimization of gear ratio will have exactly the same effect as adjustment of a winding drum radius. Nevertheless, a generator moment of inertia reflected to the cable increases proportionally to the gear ratio squared. The generator efficiency can be adjusted by selecting a different design comprising the generator and the related inverter or controller. The main limitations are maximum power and moment of inertia. The elastic coupling between winding drum and aircraft affects the system dynamics. This phenomenon should be further evaluated in frequency domain to rule out the resonance phenomenon during the arresting process. Figure 8

presents the graphs of recovered energy against gear ratio and final setup response.

Initially, the gear ratio for all subsystems was set to 3. Then, the optimization was performed for the first subsystem shown in Figure 8a. Multiple iterations were conducted with varying gear ratios. The higher gear ratio resulted in more recovered energy but increased initial deceleration caused by initial mismatch between aircraft and subsystems velocity. Hence, the gear ratio of 3.4 was chosen. Next, a similar procedure was applied for the second subsystem given in Figure 8b and third presented in Figure 8c with corresponding gear ratios of 8.4 and 20. Finally, the iterations were made for all subsystems combined, which is shown in Figure 8d. A multiplier varying between 0.7 and 1.3 was set. The results in Figure 8e indicate that peak deceleration does not exceed 2.5 m/s^2. A gear reducer with adjustable gear ratio would further increase the efficiency of the system. The different sizes of generators may also be considered where the most powerful ones could be fitted in the runway ends and smaller ones mid-runway.

6. Arresting gear energy recovery system in practice

Once the system effectiveness in energy recovery is known, more factors should be considered prior to implementation emphasizing safety. The most of accidents in aviation occurs during landing (Airbus 2022) and the arresting gear heavily influences this phase. Undoubtedly, any malfunction of this system may be catastrophic and the CS-25 standards developed for commercial operations state that any catastrophic failure condition shall be extremely improbable and not resulting from a single failure (European Union Aviation Safety Agency 2020). In contrast to aircraft carriers where successful landing is completely dependent on the arresting gear, the commercial aircraft would retain its ability to decelerate solely by using onboard systems. Consequently, emergency features such as a rapid hook release or an arresting rope cutaway would allow to rapidly disengage the device and an aircraft would continue to decelerate on its own.

Any off-axis landing poses another safety concern due to lateral force and yawing moment acting on aircraft which hardly ever land perfectly aligned with a runway axis due to environmental uncertainty and human factor. This problem is well known in military applications and Zhang et al. (2022) modeled the lateral security boundary of arresting and the landing target area for aircraft carrier operations. Similarly, the landing variability must be accounted during the system development for commercial aircraft to meet the civilian safety requirements. Since the system proposed in this paper relies on electric machines rather than hydraulics, higher safety margins can be achieved by dynamically vectoring the arresting rope tension and applying the differential kinematics for the winding drums on each side of a runway. The proposed solution is a challenge regarding the control architecture development nevertheless, the recent breakthroughs in artificial intelligence are rather optimistic. Koo et al. (2018) demonstrated the automatic unmanned aerial vehicle carrier landing using a model predictive control that considers carrier deck motion. Another concern about the control system is linked to inertia ratio between the electric machine and the load which is excessively high at proposed gear ratios. Hence, the resonance and anti-resonance peaks have a lower frequency and consequently the operational bandwidth of motor-generator is reduced, impacting the performance of the system (Knight 2021). Further investigation of dynamics is necessary where the simulation could be done with exact electric machine dynamics rather than a transfer function lag only.

An arresting cable may snap during operation due to high tensile stresses and if failure occurs, the cable will spring back potentially leading to damage of both, a landing aircraft, and airport systems. The increased lateral safety margins for landing would further intensify this issue. Egido Fern Andez, García-Fogeda Nuñez, and Arévalo Lozano (2020) investigated the fatigue life of the arresting cable and stated that the off-center arrest leads to higher stress acting on the cable.

The proposed arresting gear system design assumes that a landing aircraft will repeatedly roll over arresting cables. This situation already occurs when an airfield is used for both military and commercial operations. Accordingly, Airbus (2019) released the safety recommendations for the aircraft crossing arresting cables at speeds greater than 60 knots. Albeit they permit to roll over a rigged arresting cable, the recommendation is made to regularly check a landing gear for damage and often verify the tyre pressure.

During the standard landing, stresses are distributed between multiple deceleration systems, including friction brakes, thrust reversers and spoilers. If the arresting gear system is implemented, all forces will be translated through the arresting hook to a landing gear. Hence, an investigation of stress distribution in the aircraft landing gear and airframe is required.

Eager, Pendrill, and Reistad (2016) stated that a human body requires time to adjust a muscle tension against all acting forces. They recommended that any design interacting with a human body shall minimize the value of third position derivative with respect to time and keep the fourth close to zero. During the arresting process, the deceleration higher order derivatives peak when a landing aircraft releases a first arresting subsystem and engages with another and therefore, the passengers and cabin crew may feel discomfort during landing. The issue may be overcome by hooking two cables at once where simultaneously, the first subsystem reduces and the second increases the tension. The double cable arresting hook requires an additional mechanism which will hold both cables and allow one to be released without interference of another.

The aircraft landing direction on a runway is strictly dependent on wind, meaning that each arresting gear system should be capable of operation for either side landing. Correspondingly, a positioning of the subsystems in a runway should allow the arrest of aircraft in both directions. The runway excursion functionality of the enclosure should also be bi-directional to maximize safety of proposed system.

In busy airports, any cable maintenance or replacement required throughout a day will be highly impractical. The arresting cable is subjected to the most harsh working environment out of all components in the system due to high stress and dragging along the runway. The arrangement from Figure 1b requires a mechanical guide which will align the steel wire rope during the retraction process. The issue can be negated by using a tape instead of a steel wire rope, similar to the BAK-12 military arresting gear (Adamowicz, Poświata, and Wesołowski 2021).

The arresting device demonstrated in this paper increases landing operation redundancy and unlike the friction brakes

onboard of aircraft, it would provide the constant deceleration regardless of weather condition. The greatest safety improvement would be achieved during severe weather when the aircraft tyres have limited grip.

7. Conclusions

The energy recovery arresting gear system is a potential source of electric energy which will be even more applicable when the aerospace industry abandon fossil fuel. At that point, the system will produce completely green electrical energy and onboard storage capabilities may be used. Although there are many advantages linked to the proposed system, the practical aspects including safety, passenger comfort and life cycle of arresting components are significant, as explained in this study.

The current advancement of technology allows implementation of an arresting gear system that will recover kinetic energy and stop a civilian aircraft within the standard landing parameter values defined in the literature review. As shown in the design, five subsystems were used with a combined runout distance equal 2.5 km and each generator has maximum power of 17 MW. The system is capable of stopping one of the biggest aircraft, namely the Airbus A380, completely.

The force-based dynamic model was created according to kinematic coupling related to Hooke's law and was augmented with the energy dissipation factors such as drag and rolling resistance defined according to referenced values. The motor-generator efficiency map was a special case which contained only eight real data breakpoints while others were estimated. The simulation results demonstrated that the optimized system has approximately 60% energy conversion efficiency between aircraft kinetic energy and electrical energy.

For the medium-haul aircraft, there should be as much as 70 kWh of generated electrical energy. Using Heathrow Airport as an example application, where 650 landings took place every day in 2019 (Heathrow 2016), the kinetic energy captured via arresting gear system from all landings would generate approximately 17 GWh of electrical energy per annum, which is more than Heathrow's biomass-fueled T2 energy center produce (VAS 2021). This amount of recovered electrical energy would offset annually 5667 m^3 of diesel fuel fed into the generator which is 30% efficient, or 6367 metric tons of coal fed into a coal power plant with 33% efficiency.

This research utilized a dynamic model where each cable is considered as an ideal spring, which is an accurate representation for estimating the amount of electrical energy recovered. Nevertheless, a more realistic dynamic model has yet to be designed for a controller development purpose. This could be achieved by augmenting the dynamic model with rope mass model which will include kink waves phenomena.

Disclosure statement

No potential conflict of interest was reported by the author(s).

Funding

The work was supported by the Engineering and Physical Sciences Research Council (Grant Number 2517982) and Airbus Operations Ltd.

Data availability statement

The data that support the findings of this study are openly available in Cranfield Online Research Data (CORD) at https://doi.org/10.17862/cranfield.rd.20066996.

References

Abbas, A., J. de Vicente, and E. Valero. 2013. Aerodynamic technologies to improve aircraft performance. *Aerospace Science and Technology* 28 (1):100–32, July. doi: 10.1016/j.ast.2012.10.008.

Adamowicz, M., A. Poświata, and M. Wesołowski. 2021. Operations and maintenance of the aircraft arresting gear systems in the polish air force. Part 1. Journal of KONBiN 51 (1):105–24, March. doi:10.2478/jok-2021-0008

Airbus. 2005a. *A319 aircraft characteristics airport and maintenance planning*. Accessed August 4, 2022.

Airbus. 2005b. *A380 aircraft characteristics airport and maintenance planning*. Accessed August 4, 2022. https://www.airbus.com/sites/g/files/jlcbta136/files/2021-11/Airbus-Aircraft-AC-A380.pdf

Airbus. 2019. *Arrestor trampling of rigger arrestor cables*. Blagnac Cedex. Accessed August 15, 2022. https://www.airbus.com/content/dam/corporate-topics/publications/backgrounders/techdata/general-information/Airbus-Commercial-Aircraft-Arrestor-gear-advisory-notice-M12003945.pdf.

Airbus. 2022. A statistical analysis of commercial aviation accidents 1958 - 2021, Ref. X00D17008863 issue 6. *(Tech. Rep.)*. Blagnac Cedex. https://accidentstats.airbus.com/sites/default/files/2022-02/Statistical-Analysis-of-Commercial-Aviation-Accidents-1958-2021.pdf

Airport Technology. 2020. *Time-based separation at Heathrow: Optimised airport resilience and reducing delays*. Accessed August 10, 2021. https://www.airport-technology.com/features/time-based-separation-at-heathrow-optimised-airport-resilience-and-reducing-delays/

Anagnostopoulos, J. S., and D. E. Papantonis. 2007. Pumping station design for a pumped-storage wind-hydro power plant. *Energy Conversion and Management* 48 (11):3009–17, November. doi: 10.1016/j.enconman.2007.07.015.

Badain, N., T. Reinhart, C. Cooper, J. MacIsaac, and J. Whitefoot. 2015. Heavy-duty vehicle fuel saving technology analysis to support phase 2 regulations. *SAE International Journal of Commercial Vehicles* 8 (2):2015–01–2775, September. doi:10.4271/2015-01-2775

Barrade, P., and A. Rufer. 2004. The use of supercapacitors for energy storage in traction systems. Vehicular Power and Propulsion Symposium (IEEE-VPP 04), 6-8 October 2004, Paris, France (pp. 4–5).

The Business Research Company. 2020. *Advancements in supercapacitor technology to drive market growth*. Accessed October 2, 2021. https://blog.marketresearch.com/advancement-in-supercapacitor-technology-to-drive-market-growth

The Crosby Group. 2013. *Sheave size and wire rope strength*. Accessed May 25, 2021. https://www.thecrosbygroup.com/html/en-US/pdf/pgs/380.pdf

Department of the Navy. 2004. *NATOPS flight manual navy model F-14D aircraft*. Accessed May 6, 2022. https://info.publicintelligence.net/F14AAD-1.pdf

Eager, D., A.-M. Pendrill, and N. Reistad. 2016. Beyond velocity and acceleration: Jerk, snap and higher derivatives. *European Journal of Physics* 37 (6):065008, November. doi: 10.1088/0143-0807/37/6/065008.

Eggleston, J. 2011. *Aviation Boatswain's Mate E (NAVEDTRA 14310)*.

Egido Fern Andez, A., P. García-Fogeda Nuñez, and F. Arévalo Lozano. 2020. Vibration and fatigue life of an arresting cable under impact landing loads. *Aircraft Engineering and Aerospace Technology* 92 (8):1207–13. doi:10.1108/AEAT-10-2019-0209.

Engineering and Physical Sciences Research Council. 2019. *Delivery plan*. Accessed June 10, 2022. https://www.ukri.org/wp-content/uploads/2022/01/EPSRC-11012022-DeliveryPlan2019.pdf

Engineers Edge LLC. 2021. *Coefficient of friction equation and table chart*. Accessed August 14, 2021. https://www.engineersedge.com/coeffients_of_friction.htm

Epstein, A. H. 2014. Aeropropulsion for commercial aviation in the twenty- first century and research directions needed. *AIAA Journal* 52 (5):901–11, May. doi: 10.2514/1.J052713.

European Commission. 2011. Flightpath 2050: Europe's vision for aviation: Maintaining global leadership and serving society's needs *(Tech. Rep.)*. Publications Office. https://ec.europa.eu/transport/sites/transport/files/modes/air/doc/flightpath2050.pdf

European Parliament. 2019. *Emissions from planes and ships: facts and figures*. Accessed April 20, 2021. https://www.europarl.europa.eu/news/en/headlines/society/20191129STO67756/emissions-from-planes-and-ships-facts-and-figures-infographic

European Union Aviation Safety Agency. 2020. *CS-25 Amendment 24*. Accessed August 4, 2022. https://www.easa.europa.eu/downloads/108355/en

Feldhan, J. 2019. *Scaling battery technology*. Accessed July 3, 2022. https://semiengineering.com/scaling-battery-technology/

Fleming, G. G., and I. de Lepinay. 2019. *Environmental trends in aviation to 2050*. Accessed August 4, 2022. https://www.icao.int/environmental-protection/Documents/EnvironmentalReports/2019/ENVReport2019_pg17-23.pdf

Gleick, P. H. 2009. Three Gorges Dam Project, Yangtze River, China. *The world's water 2008–2009: The biennial report on freshwater resources*, 139–50.

Heathrow. 2016. *How to land 650 aircrafts in 1 day*. Accessed July 6, 2021. https://www.heathrow.com/latest-news/heathrow-arrivals-whats-involved-with-landing-an-aircraft-at-the-uks-busiest-airport

Heathrow Airport Ltd. 2021. *Facts and figures*. Accessed November 13, 2022. https://www.heathrow.com/company/about-heathrow/facts-and-figures

Knight, B. (2021). *Understanding inertia ratio and its effect on machine performance [White paper]*. https://us.mitsubishielectric.com/fa/en/support/technical-support/knowledge-base/getdocument/?docid=3E26SJWH3ZZR-41-13086

Koo, S., S. Kim, J. Suk, Y. Kim, and J. Shin. 2018. Improvement of shipboard landing performance of fixed-wing UAV using model predictive control. *International Journal of Control, Automation, and Systems* 16 (6):2697–708, December. doi: 10.1007/s12555-017-0690-1.

Kottas, A. T., M. N. Bozoudis, and M. A. Madas. 2020. Turbofan aero-engine efficiency evaluation: An integrated approach using VSBM two-stage network DEA. *Omega* 92:102167, April. doi:10.1016/j.omega.2019.102167.

Kumar, S. 2015. *Fuzzy logic based driving pattern recognition for hybrid electric vehicle energy management*. Unpublished doctoral dissertation, Arizona State University.

Lauk, P. (2019). *New technological solutions to improve the aerodynamic characteristics of an aircraft wing*. Doctoral dissertation, Talinn University of Technology.

Lee, D., D. Fahey, A. Skowron, M. Allen, U. Burkhardt, Q. Chen, L. Wilcox, S. Freeman, P. M. Forster, J. Fuglestvedt, et al. 2021. The contribution of global aviation to anthropogenic climate forcing for 2000 to 2018. *Atmospheric Environment* 244:117834, January. doi:10.1016/j.atmosenv.2020.117834.

Liu, F., Z. Li, H. Xie, L. Yang, and M. Hu. 2021. Predicting fuel consumption reduction potentials based on 4D trajectory optimization with heterogeneous constraints. *Sustain- Ability* 13 (13):7043, June. doi:10.3390/su13137043

Li, G., B. Yuan, M. Ge, G. Xiao, T. Li, and J.-Q. Wang. 2022. Capacity configuration optimization of a hybrid renewable energy system with hydrogen storage. *International Journal of Green Energy*:1–17, January. doi:10.1080/15435075.2021.2018323

Masiol, M., and R. M. Harrison. 2014. Aircraft engine exhaust emissions and other airport-related contributions to ambient air pollution: A review. *Atmospheric Environment* 95:409–55, October. doi:10.1016/j.atmosenv.2014.05.070.

Masuzawa, T., M. Osa, and M. Mapley. 2018. Motor design and impeller suspension. In *Mechanical circulatory and respiratory support*, ed. S. D. Gregory, M. C. Stevens, J. F. B. T. M. C. Fraser, and R. Support, 335–77. Elsevier. doi:10.1016/B978-0-12-810491-0.00011-4.

ModernAirlines. 2021. *ModernAirliners*. Accessed July 22, 2021. https://modernairliners.com/

Nord Drivesystems. 2021. *MAXXDRIVETM large industrial gear units (G1050)*. Accessed March 7, 2021. https://www.nord.com/media/documents/bw/g1050_global_5060hz_en_1-2.pdf

Openairlines. 2021. *Four questions about idle reverse thrust (white paper)*. Accessed July 8, 2021. https://blog.openairlines.com/video-best-practice-idle-reverse-thrust

Palt, K. 2019. *Flugzeug info*. Accessed July 21, 2021. http://www.flugzeuginfo.net/index_en.php

Rabbat, B. G., and H. G. Russell. 1985. Friction coefficient of steel on concrete or grout. *Journal of Structural Engineering* 111 (3):505–15, March. doi: 10.1061/(ASCE)0733-9445(1985)111:3(505).

RotableRepairs. 2021. *A320 aircraft wheel, brake and tyres supported*. Accessed May 23, 2021. https://www.rotablerepairs.com/a320-airbus.html

Rustenburg, J. W., D. A. Skinn, and D. O. Tipps. (2002). Statistical loads data for the airbus A- 320 aircraft in commercial operations. *(Tech. Rep.)*. University of Dayton Research Institute. http://www.tc.faa.gov/its/worldpac/techrpt/ar02-35.pdf

Safran. 2017. *Electric taxiing*. Accessed April 25, 2021. https://www.safran-landing-systems.com/systems-equipment/electric-taxiing-0

Siemens. 2021. *Siemens simotics HV M*. Accessed May 28, 2021. https://new.siemens.com/global/en/products/drives/electric-motors/high-voltage-motors/simotics-hv-m.html

Song, Z., J. Li, J. Hou, H. Hofmann, M. Ouyang, and J. Du. 2018. The battery- supercapacitor hybrid energy storage system in electric vehicle applications: A case study. *Energy* 154:433–41, July. doi:10.1016/j.energy.2018.04.148.

Steilen, M., and L. Jörissen. (2015). Hydrogen conversion into electricity and thermal energy by fuel cells. In *Electrochemical energy storage for renewable sources and grid balancing*, eds. P. T. Moseley, J. B. T. E. E. S. F. R. S. Garche, and G. Balancing, 143–58. Amsterdam: Elsevier. doi:10.1016/B978-0-444-62616-5.00010-3

Sun, J., J. M. Hoekstra, and J. Ellerbroek. 2020. Estimating aircraft drag polar using open flight surveillance data and a stochastic total energy model. *Transportation Research Part C: Emerging Technologies* 114:391–404, May. doi:10.1016/j.trc.2020.01.026.

SWR. 2021. *6x36 (14/7+7/7/1) - IWRC Wire Rope*. Accessed May 25, 2021. https://www.steelwirerope.com/WireRopes/Galvanised/6x36-IWRC-wire-rope.html

TaxiBot. 2021. *TaxiBot*. Accessed April 25, 2021. https://www.taxibot-international.com/

Tomaszewska, A., Z. Chu, X. Feng, S. O'Kane, X. Liu, J. Chen, B. Wu, E. Endler, R. Li, L. Liu, et al. 2019. Lithium-ion battery fast charging: A review. *eTransportation* 1:100011, August. doi:10.1016/j.etran.2019.100011.

United Nations. 2022. *Progress towards the sustainable development goals report of the secretary- general*. Accessed June 6, 2022. https://sustainabledevelopment.un.org/content/documents/29858SG_SDG_Progress_Report_2022.pdf

VAS. 2021. *Biomass plant heathrow airport*. Accessed September 15, 2021. https://www.vas.co.at/de/biomass-plant-heathrow-airport/

Vestas. 2021. *V236-15.0 MW*. Accessed October 5, 2021. https://www.vestas.com/en/products/offshore-platforms/v236_15_mw#!grid_0_content_0_Container

WheelTug. 2021. *WheelTug*. Accessed April 25, 2021. https://www.wheeltug.com/

Wu, M. C., D. Kamensky, C. Wang, A. J. Herrema, F. Xu, M. S. Pigazzini, M.-C. Hsu, A. L. Marsden, Y. Bazilevs, M.-C. Hsu. 2017. Optimizing fluid–structure interaction systems with immersogeometric analysis and surrogate modeling: Application to a hydraulic arresting gear. *Computer Methods in Applied Mechanics and Engineering* 316:668–93, April. doi:10.1016/j.cma.2016.09.032.

Yager, T. J., S. M. Stubbs, and P. A. Davis. 1990. Aircraft radial-belted tire evaluation. *SAE Transactions* 99:1752–59, May. http://www.jstor.org/stable/44473143.

Yang, M., J. Yang, and H. Ding. 2018. A two-stage friction model and its application in tracking error pre-compensation of CNC machine tools. *Precision Engineering* 51:426–36, January. doi:10.1016/j.precisioneng.2017.09.014.

Yilmaz, N. 2022. Comparative energy and environmental assessment of battery technologies and alternative fuels in sustainable aviation. *International Journal of Green Energy*:1–10, May. doi:10.1080/15435075.2022.2075226

Zhang, Z., Y. Peng, T. Liang, X. Wei, and Y. Wang. 2022. Research on lateral dynamics safety margins of carrier-based aircraft arresting. *Aeronautical Journal*:1–23, February. doi:10.1017/aer.2022.1

Zolkin, A. L., S. A. Galanskiy, and A. M. Kuzmin. 2021. Perspectives for use of composite and polymer materials in aircraft construction. *IOP Conference Series: Materials Science and Engineering* 1047 (1):012023, February. doi: 10.1088/1757-899X/1047/1/012023.

Zsiborács, H., N. H. Baranyai, A. Vincze, L. Zentkó, Z. Birkner, K. Máté, and G. Pintér. 2019. Intermittent renewable energy sources: The role of energy storage in the European power system of 2040. *Electronics* 8 (7):729, June. doi: 10.3390/electronics8070729.

Appendices

Appendix A

A.1

Cross-section view of winding subsystem

BALLOON NO.	DESCRIPTION	QTY
1	FOUNDATION	1
2	MOTOR-GENERATOR	1
3	GEAR REDUCER	1
4	ELECTRICAL CABINET	1
5	SERVICE ENGINEER FOR SCALE	1
6	BOTTOM BEARING (NOT VISIBLE)	1
7	BLANKING PLATE	1
8	TOP BEARING (NOT VISIBLE)	1
9	SAFETY ENCLOSURE	1
10	WINDING DRUM	1
11	ARRESTING ROPE/TAPE	1

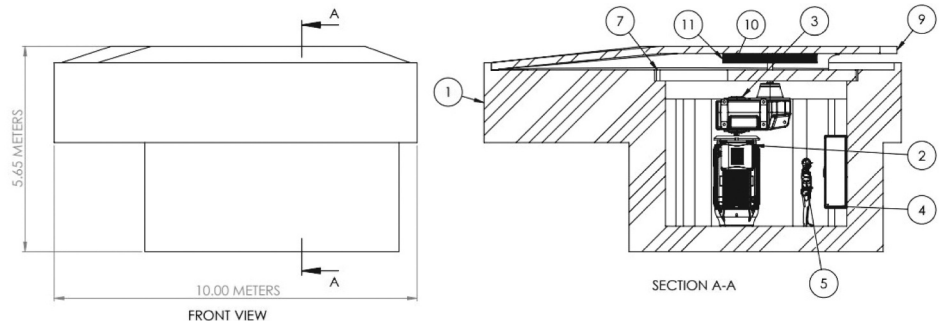

A.2

Rope against a runway coefficient of friction

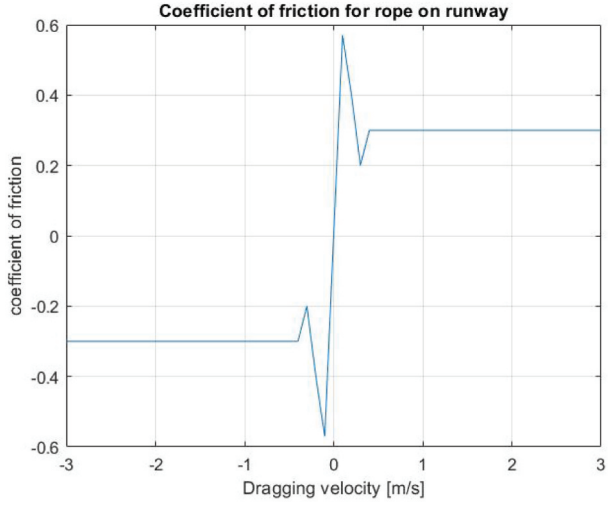

Appendix B

Rope parameters used in USS navy Mark 7 Mod 3 arresting gear systems

	Deck Pendant	Purchase Cable
Type	6x30 flat strand polyester core	6x31 flat strand polyester core
Diameter	36 mm	36 mm
Breaking strength	93 metric tons	98 metric tons

Appendix C

C.1

Generated Energy for all aircraft at gear ratio equal 3

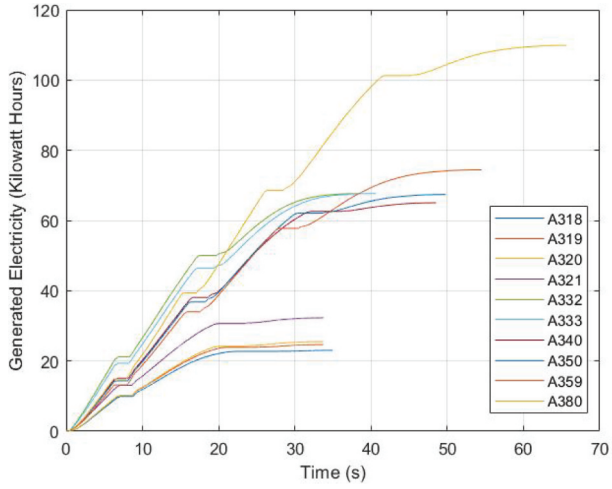

C.2

Stopping distance for all aircraft at gear ratio equal 3

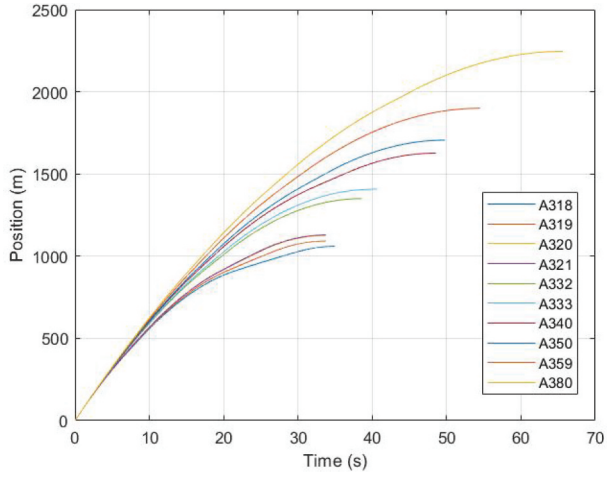

Modelling and performance evaluation of sustainable arresting gear energy recovery system for commercial aircraft

Deja, Jakub

2022-11-21

Deja J, Dayyani I, Skote M. (2023) Modelling and performance evaluation of sustainable arresting gear energy recovery system for commercial aircraft, International Journal of Green Energy, Volume 20, Issue 10, 2023, pp. 1086-1100

https://doi.org/10.1080/15435075.2022.2143715